Laser line shape recovery system based on a double pixelated axilens

Luis A. González, MEMBER SPIE
Universidad de Sonora
Departamento de Investigación en Física
Apdo. Postal 5-88
Hermosillo, Son, 83000
México

Victor Arrizón
Instituto Nacional de Astrofísica
Optica y Electrónica
Apdo. Postal 51 y 216
Puebla, Puebla 72000
México

Abstract. We describe a scanning system for shape recovery that employs a pair of one-dimensional interlaced axilenses encoded onto a reflective liquid-crystal spatial light modulator. The design of these axilenses with opposite depth presets allows the generation of a high-quality laser line pattern with extended depth of focus, which is applied in the shape recovery. Other attributes of the system allow the scanning of objects whose lateral dimensions are larger that those of the spatial light modulator itself. The high performance of the scanning system is demonstrated by its application to the shape recovery of ceramic objects.
 [DOI: 10.1117/1.3116704]

Subject terms: pixelated axilens; long depth of focus; spatial light modulator; Fresnel diffraction; 3-D shape recovering.

Paper 080920R received Nov. 24, 2008; revised manuscript received Feb. 3, 2009; accepted for publication Feb. 10, 2009; published online Apr. 14, 2009.

1 Introduction

Laser line scanning is a simple technique used to obtain three-dimensional (3-D) information by calculating the deformation of a laser line projected on the surface of a sample object.[1,2] The local line displacement is obtained by determining the highest-intensity position with peak detection algorithms. A complete scan is usually achieved by laterally shifting the object with motorized translation stages. Some systems of this type use refractive cylindrical lenses to generate the laser line pattern. Thus, due to the reduced depth of focus of these devices, the shape recovery of thick samples requires an additional axial scanning.

Recently, we reported preliminary results on the use of a 1-D axilens encoded onto a pixelated liquid crystal (LC) on a silicon spatial light modulator (SLM), which was referred to as a *pixelated axilens* (PA), for shape recovery applications.[3] A laser line with a sufficiently long focal depth, generated by this PA, enables the shape recovery without necessity of axial scanning. The lateral scanning is easily performed in this system by modulating the PA transmittance by a linear phase with variable slope, avoiding the use of moving parts or motors.

A drawback of this shape recovery system is that its scanning area is limited to the dimensions of the employed SLM. On the other hand, the sharpness of the laser line is acceptable only over a short length along the axial direction, allowing only the recovery of 3-D profiles with reduced depth.

Here, we show a significant improvement of the optical system reported in Ref. 3. The modified system is based on the encoding of two interlaced 1-D PAs with opposite focal depth presets, whose positions are interchanged in time. In order to maintain the integrity of the line pattern, subject to relatively large lateral displacements, we encoded 1-D PAs with large f numbers. With this modification it is possible to move away the secondary foci produced by the pixelated structure of the SLM to perform the shape recovery of objects larger than the dimensions of the LC SLM. In addition, stretching of the laser line pattern employed in the scanning process was achieved by placing a cylindrical lens in front of the interlaced PA. The time-average intensity of the resulting laser line pattern projected on the object is detected with a CCD camera, which is placed in a triangulation configuration.

2 Fresnel Field of a Pixelated Axilens

The analysis of the focal field produced by a 1-D axilens, based on the Fresnel diffraction approximation, was presented by Ye et al.[4] For the specific application to be discussed here, it is required to describe the properties of the focal field produced by a 1-D axilens with pixelated structure. We assume that the transmittance of a 1-D PA, implemented with a pixelated SLM, has the discrete structure depicted in Fig. 1, where ϕ_n denotes the phase delay provided by the PA pixel with the index n that takes integer values in the interval $[-Q,Q]$. It is assumed that the pixels of the PA, which have a common width a, are centered at positions $x_n=np$, where p is the pitch distance. The transmittance of the PA can be expressed as

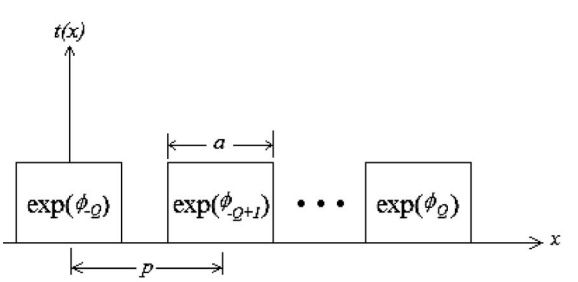

Fig. 1 Transmittance of a 1-D pixelated axilens.

$$t(x) = \sum_{n=-Q}^{Q} \exp[i\phi_n] w(x - np), \tag{1}$$

where $w(x)$ is the rectangular window of a single pixel, given by

$$w(x) = \mathrm{rect}(x/a). \tag{2}$$

The Fresnel field produced at the distance z, when a unitary plane wave of wavelength λ illuminates the PA, is calculated with the 1-D Fresnel diffraction integral as

$$U(x;z) = \frac{1}{\sqrt{\lambda z}} \exp\left[\frac{i\pi x^2}{\lambda z}\right] \sum_{n=-Q}^{Q} \exp[i\phi_n] \int_{-\infty}^{\infty} w(u - np) \times \exp\left[\frac{i\pi u^2}{\lambda z}\right] \exp\left[\frac{-i2\pi ux}{\lambda z}\right] du. \tag{3}$$

Taking into account that the width a of the pixel window is small compared to the propagation distance z, Eq. (3) is reduced to

$$U(x;z) = \frac{a}{\sqrt{\lambda z}} \exp\left[\frac{i\pi x^2}{\lambda z}\right] \sum_{n=-Q}^{Q} \exp[i\phi_n] \times \exp\left[\frac{i\pi n^2 p^2}{\lambda z}\right] \exp\left[\frac{-i2\pi xnp}{\lambda z}\right] \times \sin c\left[\frac{a}{\lambda z}(x - np)\right]. \tag{4}$$

Although Eq. (4) can be used to compute the Fresnel field of a diffractive optical element (DOE) with arbitrary phase distribution, we consider only the phase modulation of a PA. The phase function of an axilens was formerly proposed by Davidson et al.[5] as a circularly symmetric function. For our purpose, it is convenient to employ the 1-D version of this phase function, given by

$$\phi(x) = -\frac{\pi x^2}{\lambda f(x)}. \tag{5}$$

In this relation, $f(x)$ is a function that represents a spatially dependent focal length, defined as

$$f(x) = f_0 + \frac{\Delta F x^2}{R^2}, \tag{6}$$

where f_0 corresponds to the focal length produced by the central zone of the 1-D axilens, ΔF denotes a focal depth preset, and R is the radius of the axilens pupil. In order to encode the phase distribution of an axilens into a pixelated structure, we employ the sampled values of $\phi(x)$, with sampling period p, given by

$$\phi_n = -\frac{\pi n^2 p^2}{\lambda f_0 + \lambda \Delta F n^2 p^2 / R^2}. \tag{7}$$

The index n in Eq. (7) takes values in the interval $[-n_{\max}, n_{\max}]$, where $n_{\max}$ is the integer part of R/p. The transmittance of the PA is completely defined by substituting Eq. (7) into Eq. (1). A PA employed in 3-D shape recovery requires a focal intensity distribution with an axial depth as large as the height of the object to be scanned. In the definition of the PA, the introduction of a focal length $f(x)$ dependent on the pixel position x is intended to enlarge the focal depth.

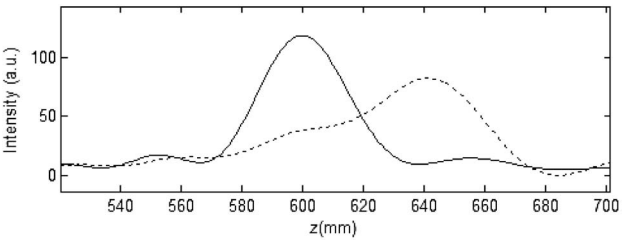

Fig. 2 Axial intensity of the main focus generated with a 1-D PA with a=15 μm, p=20 μm, λ=632.8 nm, f_0=600 mm, and N=341, when Δf=0 (continuous curve) and Δf=50 mm (dashed curve).

To illustrate the true performance of a PA, we computed the focal field of one of these devices assuming a pixel pupil a=15 μm and a pixel pitch distance p=20 μm, considering an illuminating beam of wavelength λ=632.8 nm. Other design parameters of this PA are f_0=600 mm and N=341. If a focal depth preset ΔF=0 is assumed, the phase function of the PA reduces to the transmittance of a cylindrical lens [see Eq. (7)], which produces an axial intensity with relatively small depth of focus. This axial intensity, which is maximum at the focal plane $z=f_0$, is plotted with the solid line in Fig. 2. If ΔF is increased, the phase distribution of the PA is composed of zones with different focal lengths. In Fig. 2 (dashed curve) we show the axial intensity produced by the PA under study for ΔF=50 mm. Although this intensity shows significant levels in an extended axial focal zone, its uniformity is not satisfactory.

Another important fact to consider is that in general a PA generates secondary laterally shifted foci, in addition to the main focus. Such secondary foci, which are due to the sampling of the PA transmittance, appear centered at positions $q\lambda z/p$ (for integer q). It is shown in Sec. 3.2 that the relative intensity of the secondary foci is directly dependent on the PA fill factor d/p. The computed main focus at the plane with maximum axial intensity (z=641 mm) for the PA specified is depicted in Fig. 3 together with two secondary foci.

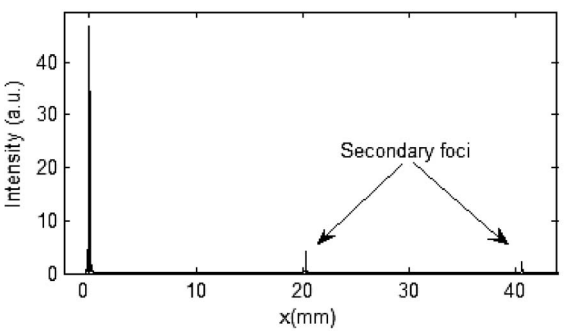

Fig. 3 Intensity distribution at the plane of maximum axial intensity, shown in Fig. 2, for the PA with Δf=50 mm.

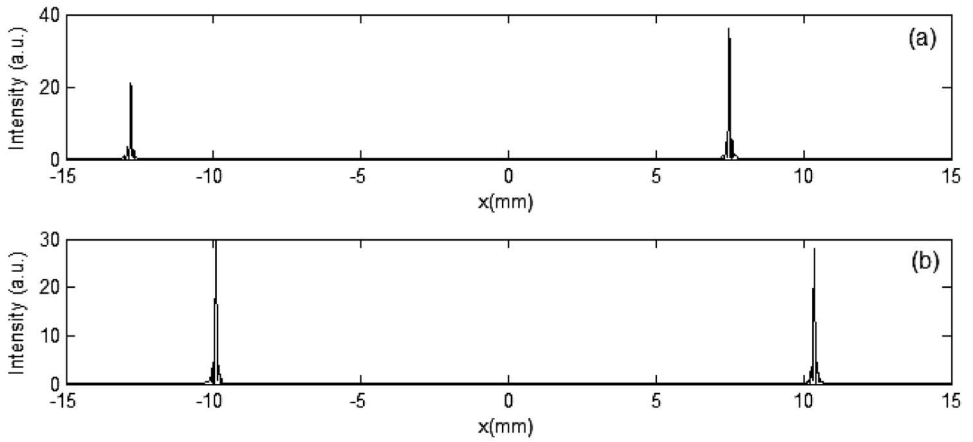

Fig. 4 View of the main and a secondary focus generated by the PA described in Fig. 2, when it is modulated by a linear phase function that enables a displacement of foci by (a) 350 pixels and (b) 485 pixels. The main focus appears at the right side in each case.

A 1-D PA similar to the one discussed was used to generate a luminous line pattern for the shape recovery of 3-D objects in Ref. 3. Although an increase of ΔF results in enlargement of the focal depth produced by this PA, the useful axial working distance for the scanning process is limited by the axial intensity variations. By the encoding of this PA, the appropriate scanning of an object with a maximum height of 6 mm was achieved in Ref. 3. On the other hand, the lateral scanning of the object is obtained by encoding PAs modulated with a dynamically modified linear phase distribution. The scanning is performed in the direction perpendicular to the axis of the focal line pattern. However, as the main focus moves away from its central position, the intensity of the close secondary focus increases and that of the main focus reduces. This fact is illustrated in Fig. 4 for the PA discussed in the previous paragraph, when it is modulated by linear phases that introduce displacements of 350 and 485 pixels, respectively. The presence of a near secondary focus is undesirable for shape recovery based on the use of a single laser line, because the lateral scanning space is significantly reduced. In the work reported in Ref. 3, this restriction confined the scanning of objects to reduced height data and lateral dimensions similar to those for the SLM that encodes the PA.

3 Improving the Scanning Process with a Reconfigurable PA

3.1 *Improving the Focal Depth*

Numerical simulations reported in Sec. 2 proved that a 1-D PA generates a focal field with an extended depth in comparison with a pixelated lens (PL) of similar parameters. However, the axial uniformity of the focal field generated by a single PA is relatively poor. In order to improve the intensity uniformity of this focal field, we propose to display simultaneously in the SLM two interlaced 1-D PAs with common focal length f_0 but opposite focal depth presets. The configuration of the composed device, which is here referred to as *double PA*, is depicted in Fig. 5. As noted in this figure, the two PAs occupy respectively the odd and the even rows of pixels in the SLM. Note that the direction where the interlacing occurs (vertical in Fig. 5) is perpendicular to the direction of the PAs' modulation (horizontal in Fig. 5). Taking advantage of the SLM's programmability, the positions of the two displayed PAs are interchanged between successive video frames. The black and white rows at the left side of Fig. 6 represent a video frame

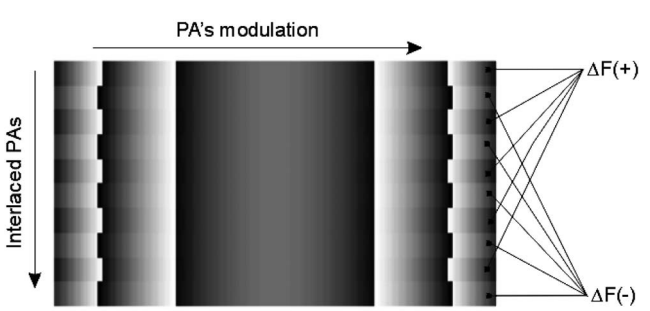

Fig. 5 Representation of a composed device formed by interlaced PAs with opposite focal depth presets.

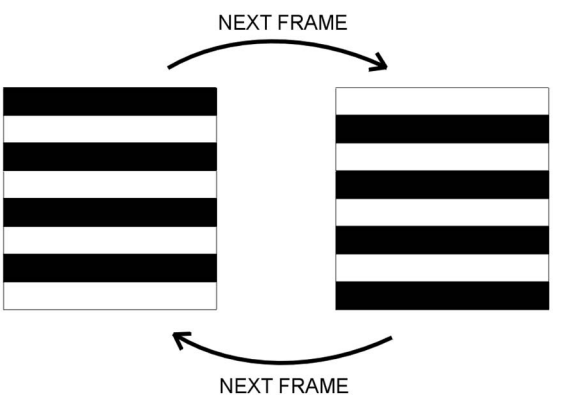

Fig. 6 Interchanging 1-D PAs with positive and negative Δf, represented by black and white rows, respectively.

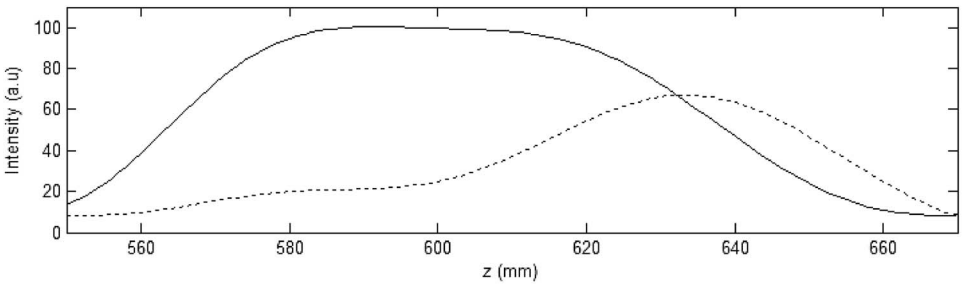

Fig. 7 Axial intensity of the main focus generated with a conventional PA (dashed curve) and a double PA (continuous curve).

with a pair of 1-D PAs with positive and negative focal depth presets, respectively. In the next video frame, represented at the right side of Fig. 6, the positions of these PAs appear interchanged. This process is repeated at video frequency to get a luminous line pattern by time-integrating the intensity of the resulting luminous patterns generated by the PAs. It is confirmed by numerical and experimental tests that the intensity uniformity of the resulting luminous line pattern is improved within an extended axial range.

As an illustrative example we calculated the integrated axial intensity produced by a double PA whose individual PAs have the following parameters: $N=330$ pixels, $f_0=600$ mm, and focal depth presets of 20 and -20 mm, respectively. The axial intensity of the double PA, plotted with a continuous curve in Fig. 7, shows a relatively high uniformity within an axial range of about 40 mm, which corresponds to the difference of the depth preset values of the individual PAs. This improvement of axial uniformity in relation to the one provided by a single PA with a depth preset of 40 mm (dashed line in Fig. 7) is remarkable.

The double PA described was experimentally implemented employing a Holoeye LC-R-2500 reflective SLM, with a pixel pupil of 17.6 μm and pixel pitch of 19 μm. The SLM, illuminated with a collimated HeNe laser ($\lambda=632.8$ nm), was addressed by a digital video interface (DVI) board attached to a TB-4V-LX25 board from HighTech Global. Video drivers and SLM pixel addressing were implemented with the field-programmable gate array of this board. Since the LC-R-2500 is a twisted-nematic-LC SLM, its modulation parameters were adjusted to achieve a phase modulation range close to 2π rad with a minimized amplitude modulation, according to the method reported in Ref. 6. The intensity distribution of the resulting laser line pattern was captured by a CCD, configured to operate with an exposure time of 0.5 s (30 video frames of our SLM), at the planes $z=580$, 600, and 620 mm. In Fig. 8 we see that, in agreement with the simulations, the experimental laser line patterns at the different planes show very similar peak intensities. Objects with heights up to 40 mm can be conveniently scanned with this device. However, other combinations of 1-D PAs can provide larger depth of focus.

3.2 *Extending the Scanning Region*

We have found, by means of numerical simulations, that the positions and relative intensity of the main and secondary foci produced by a 1-D PA basically correspond to those of foci generated by a PL with the focal length f_0 of the PA. It is well known that the lateral positions of multiple foci generated by a PL are $x_n=n(\lambda f_0/p)$.[7] On the other hand, it has been shown[8] that the normalized amplitude of the multiple foci is approximately limited by the envelope

$$e(x)=\mathrm{sinc}\left(\frac{ax}{\lambda f_0}\right)\otimes\alpha(x), \tag{8}$$

where $\alpha(x)$ is the PL pupil and the symbol $\otimes$ denotes the convolution operation. Now, assuming that f_0 is large enough, the envelope can be approximated by $e(x)=\mathrm{sinc}(ax/\lambda f_0)$. A consequence of this result is that the nor-

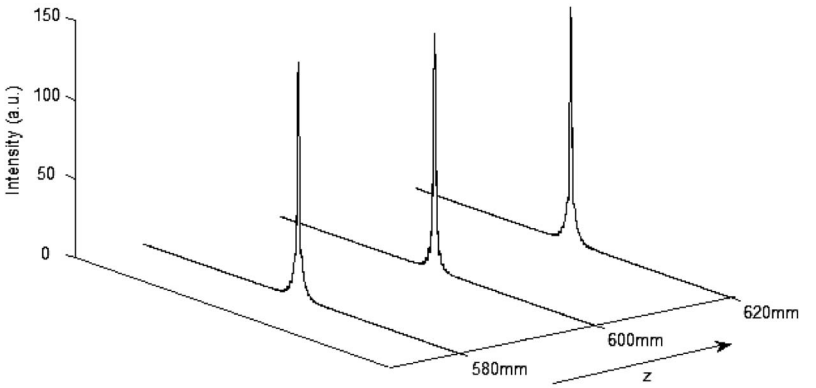

Fig. 8 Transverse intensity profiles of the main focus obtained at different planes from a double PA experimentally implemented with a LC SLM.

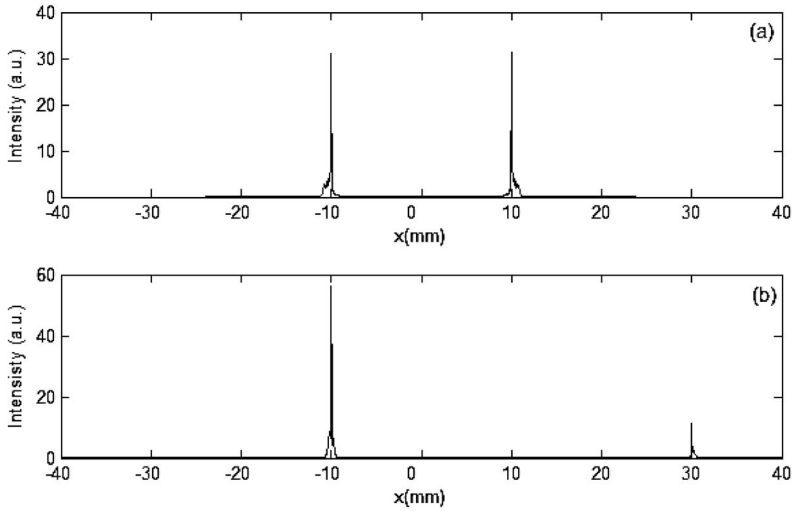

Fig. 9 Intensity profile of the main focus and the first-order secondary focus generated by a PA modulated by a linear phase function that generates a displacement of 10 mm, employing f numbers of (a) $f_{\#}=41$ and (b) $f_{\#}=82$.

malized amplitude of the first-order secondary focus ($n=1$), given by $\mathrm{sinc}(a/p)$, is dependent only on the SLM fill factor a/p. On the other hand, it can be readily shown that the distance of the secondary focus ($n=1$) from the main focus ($n=0$) is $\Delta x=N\lambda f_{\#}$, where N and $f_{\#}$ are respectively the number of pixels and the f number of the PL. Thus, the separation of the first lateral focus (and therefore the lateral scanning space enabled by the device) can be increased either increasing the number of pixels (N) or the device f number $f_{\#}$. For the PA's implemented with the available SLM (LC-R-2500) we employ a fixed number $N=768$, which corresponds to the number of pixels in one of the SLM directions.

As an example, we computed the transverse intensities at the focal plane of 1-D PAs with f numbers of 41 ($f_0=600$ mm) and 82 ($f_0=1200$ mm) modulated by a linear phase function to achieve a displacement of -10 mm at the lateral position of the main focus. A portion of the resulting intensity distribution at the focal plane f_0 for both PAs is plotted in Fig. 9(a) and 9(b), respectively. Only the main (left) and first-order (right) foci are shown in each case. Since the distance between foci is proportional to the focal distance, we can observe a larger separation distance between the main and secondary foci for the PA with larger $f_{\#}$. One of the drawbacks of the PA with small $f_{\#}$ is the significant attenuation of the main focus, together with the amplitude increase of the secondary focus. In general we can observe that the attenuation of the main focus under a displacement D_x increases with the ratio D_x/D_{sf}, where D_{sf} is the distance of secondary focus from the main focus. Figure 9(a) illustrates that for the PA with $f_{\#}=41$ the two foci have similar intensities when $D_x=20$ mm and $D_{\mathrm{sf}}=20$ mm. If we apply the same displacement to the PA with $f_{\#}=82$, the resulting main focus shows a smaller attenuation with respect to its corresponding secondary focus. The shape recovery of objects can be performed with such PAs by selecting a rectangular section on the image acquired by a CCD camera to isolate the image of the main focus. As an illustration, dashed lines in Fig. 10(a) show the limits of a rectangular section that isolate the intensity of the main focus from the secondary focus projected over a simulated object. If the displacement produced by the shape of the object is higher than the separation of adjacent foci, the isolation of the main focus is difficult because the scanning scene shows multiple foci [see Fig. 10(b)]. The use of PAs with large $f_{\#}$ facilitates the isolation of the multiple deformed focal lines introduced by several secondary foci.

4 3-D Shape Recovery with the Scanning System

4.1 *Shape Recovery Method*

A schematic setup of the laser line generator used to scan the shape of the objects with the modifications described in Sec. 3 is shown in Fig. 11. A collimated laser beam is used to illuminate the modulation stage of the system, formed by an input polarizer (IP), a quarterwave plate (QWP), the reflective SLM, and an output polarizer (OP). In order to achieve a larger working length in the direction perpendicular to both the z axis and the scanning direction, we employ a refractive cylindrical lens at the output of the laser line

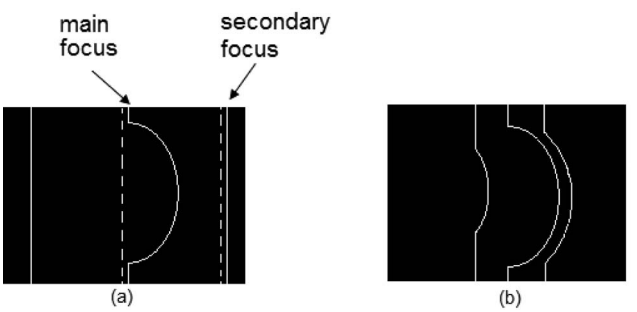

Fig. 10 Schematic illustration of the deformed main and first-order focal lines when deformations are (a) smaller and (b) larger than the distance of the first-order focal line.

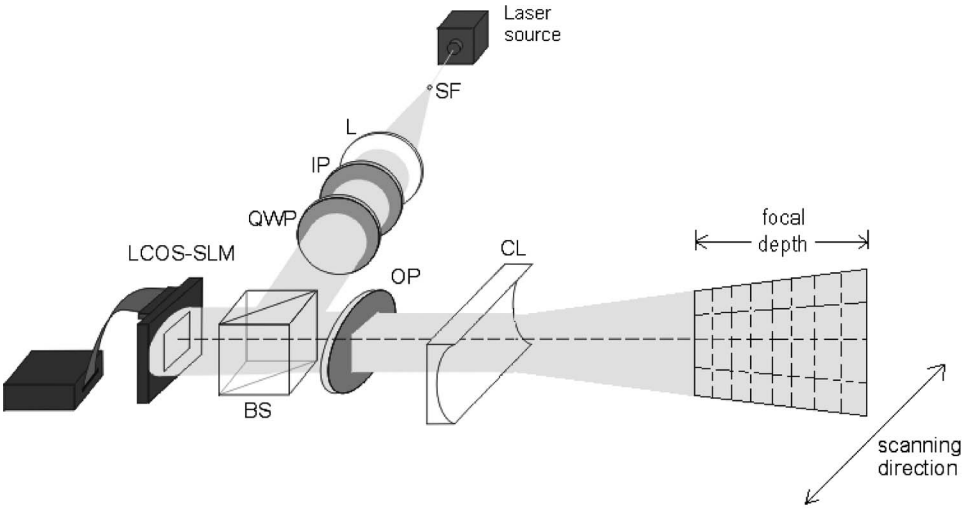

Fig. 11 Setup of the laser line generator based on the encoding of double PAs with a LC-on-Si SLM.

generator to produce a stretching of the laser line pattern. The stretching ratio depends on the distance of the cylindrical lens from the PA.

The scheme of the shape-recovering system is shown in Fig. 12, where H and d are the distances from the reference plane and the laser line generator, respectively, to the CCD camera, and $h(x)$ is the height of the object's surface with respect to the reference plane. Shape recovery of 3-D objects can be performed with this setup by means of optical triangulation. A relationship to calculate the height data $h(x)$ of the object from the displacement of the projected laser line can be obtained from the geometry of Fig. 12. The shape of the object placed on the reference plane shifts the projected laser line from x_1 to x_2. In such a case $h(x)$ is calculated as[9]

$$h(x) = \frac{Hs(x)}{d + s(x)}, \tag{9}$$

where $s(x)$ is the distance between the data points x_1 and x_2, which are determined by the position of the peak intensity

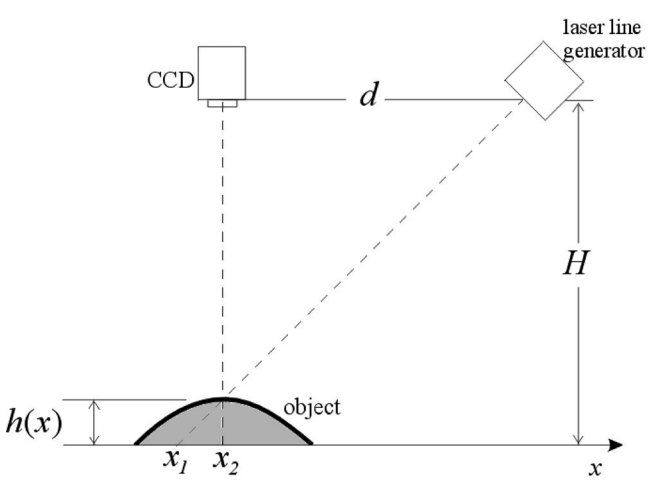

Fig. 12 Optical geometry of the shape recovery system.

of the laser line pattern on the x axis. Prior to a peak detection algorithm, a lowpass filter is applied to the resulting image detected by the CCD to attenuate the influence of the speckle pattern (or high-frequency intensity variations).

The peak detection algorithm is based on a direct search for the maximum intensity over the rows of the resulting image. When a row of the image is chosen, the following steps are performed:

1. Select the value of the first element from a row of the image [elem(1)] as the reference value (ref_val), and its index $k=1$ as the pixel position of the element (pixel_loc).
2. The index k is increased by one, and the next element elem(k) of the row image is selected.
3. If the value of the selected element is larger than ref_val, then pixel_loc=k and ref_val=elem(k).
4. Steps 2 and 3 are repeated until all the elements of the row are read. This process returns the index of the element with the maximum value.

The shape of the object is then recovered by comparing the positions of the luminous peak produced by the laser line on the sample object with those projected on the reference plane (a flat plate).

4.2 *Experimental Implementation*

In order to perform the scanning of 3-D objects, 1-D double PAs of 768 pixels with focal depth presets of ± 23 mm and starting focal length $f_0=1500$ mm were dynamically encoded onto the LC-R-2500 SLM according to the approach described in Sec. 3.1. A laser line pattern with an improved focal depth of approximately 60 mm was achieved. Since the objects to be measured are placed at an inclination angle of 45 deg with respect to the axis of the laser line generator, the system has the capability to recover the shape of objects with a maximum height of 42 mm. Displacement steps of 95 μm were used to scan the objects with the main laser line pattern.

The first example is the shape reconstruction of the ceramic toy shown in Fig. 13(a). As an example of the scan-

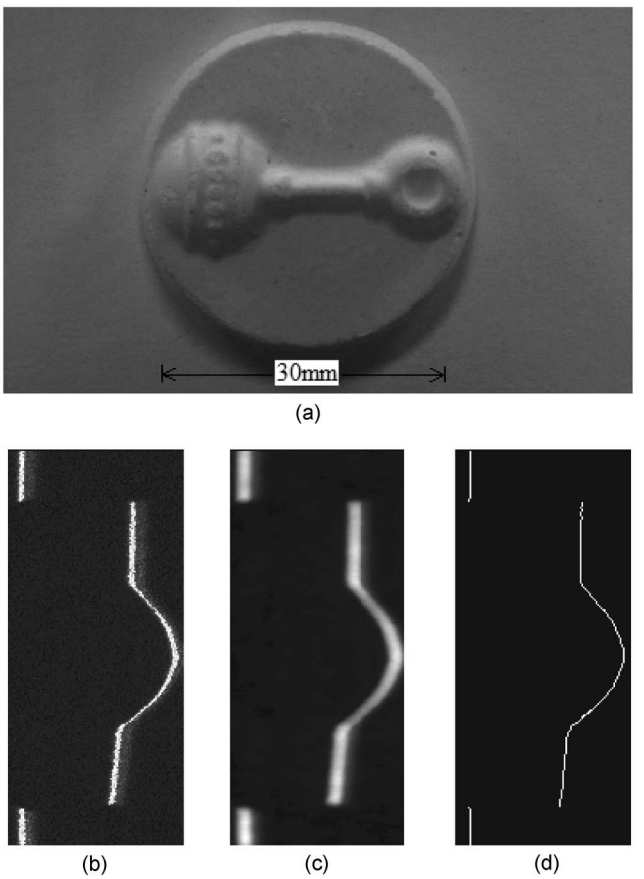

Fig. 13 (a) Image of a ceramic toy employed in the first experimental line scanning process. A typical deformed line pattern formed on the object (b) is subjected to a lowpass filter to produce a clean image (c), which is subjected to the peak detection algorithm to obtain the deformation (d).

ning process, Fig. 13(b) shows an image of a projected laser line pattern over the object. Afterwards, the image of this luminous pattern is processed with a lowpass filter [see Fig. 13(c)] and used as the input of the intensity peak detection algorithm. Figure 13(d) shows a plot of the positions of the intensity peaks (or skeleton) used to calculate the displacement $s(x)$ produced by the surface topography of the object. Then $s(x)$ is used to calculate the height data of the object, which for this example are plotted in Fig. 14. The maximum height of this object is about 13 mm. The height data are then placed on the corresponding positions

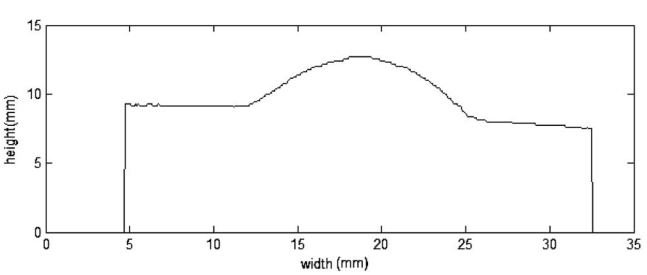

Fig. 14 Profile of the ceramic toy, showing the maximum height data obtained with the shape recovery system.

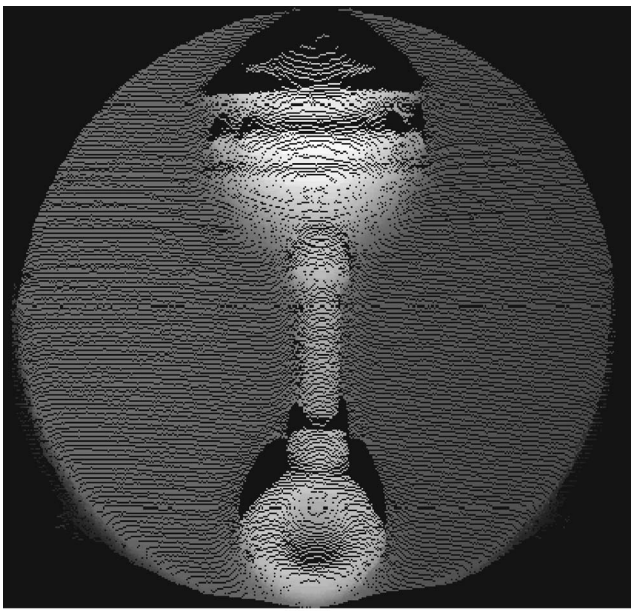

Fig. 15 Computer-based shape reconstruction of the ceramic toy.

previously established by the intensity peak detection algorithm to reconstruct the 3-D object. The scanning space required for this object was about 30 mm. Figure 15 shows an image of the reconstructed object, whose relief is represented in gray-level curves. Observe that the image of the reconstructed object shows the absence of some height data as consequence of occlusion. For the calculations of this example, we treated the occlusion zones as null (zero-height) data.

As a second example, the shape recovery of a face from the ceramic model shown in Fig. 16(a) was performed. As a result of the shape-recovering process, in Fig. 16(b) we show a computer reconstruction of the object represented with grayscale curves. Figure 16(c) shows a sample of the measured heights along the object, with a maximum height of approximately 30 mm. If the surface of the object has smooth variations, zones with absent height data produced by occlusion can be treated with interpolation methods. Figure 16(d) shows a portion of the object under study reconstructed by interpolating the surface data according to the method reported in Ref. 9 In general, it is observed that the computer reconstructions show the shape features of the original objects. Thus, this approach can be considered as a good alternative method for the shape recovery of objects.

5 Final Remarks and Conclusions

LC SLMs are devices conveniently used to encode multiple phase functions. Moreover, the electrical addressability of these devices allows the generation of time-changing luminous patterns. We used this advantage to improve the performance of a shape recovery system by using a LC SLM to encode double 1-D PAs. As a result of interchanging the positions of the single 1-D PAs between frames of the SLM according to the method described in Sec. 3, a laser line pattern with larger depth of focus than that generated by a single PA was obtained. Although the scanning system was used to recover the shape of objects up to 30 mm, other

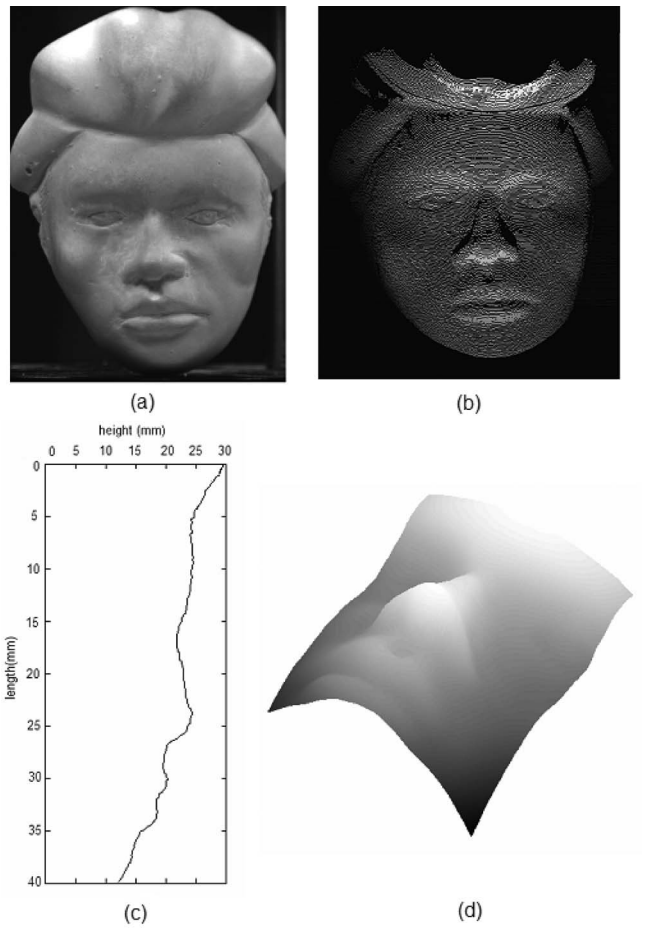

Fig. 16 Reconstruction of the ceramic model of a face: (a) object, (b) view of the computer shape reconstruction of the object, (c) profile of the object, and (d) partial 3-D view of the reconstructed face using an interpolation algorithm.

combinations of double PAs can be used to scan objects with larger heights. Moreover, it is also possible to employ three or more interlaced 1-D PAs for a further improvement of the extended focal depth. In this case, SLMs with faster response and addressing will be needed. Besides the proposal reported in this paper, different reported techniques to extend the depth of focus[10,11] could be explored and adapted for scanning systems.

In order to obtain an appropriate scanning window with a single laser line, we achieved the separation of the secondary foci (produced by the pixelated structure of the SLM) by encoding PAs with large f numbers. According to the analysis of Sec. 3.2, the separation of secondary foci from the main focus is $N\lambda f_{\#}$. From this analysis, it is also seen that the scanning of objects could be done using smaller focal distance if a LC SLM with smaller pixels and high fill factor is employed. The profile measurement resolution with conventional shape recovery systems depends firstly on the step resolution provided by the motors used to move the object. In contrast, continuous displacements of the laser line pattern from continuous displacements of the encoded PAs can be produced with our system. Therefore, with this approach the profile measurement resolution depends only on the camera sensor element and the optical magnification.

In summary, the modified scanning system using double interlaced PAs enables the appropriate scanning of objects with increased dimensions (both height and lateral size), in comparison with the original system, which only employs single PAs. Although the scanning system of this studio was developed for the shape reconstruction of objects, applications such as robotic vision and bar code readers can be conveniently performed as well.

Acknowledgment

This work was financially supported by the Consejo Nacional de Ciencia y Tecnología (CONACyT), México, under project 44071-A1.

References

1. W. C. Tai and M. Chang, "Noncontact profilometric measurement of large-form parts," *Opt. Eng.* **35**(9), 2730–2735 (1996).
2. L. P. Thomas, R. Gratton, B. M. Marino, and J. M. Simon, "Measurements of free surface profiles in transient flow by a simple light slicing method," *Appl. Opt.* **33**(13), 2455–2458 (1994).
3. L. A. González, V. Arrizón, and A. Vera-Marquina, "Programmable pixelated lens with long depth of focus for shape recovering applications," *Proc. SPIE* **6311**, 63110V (2006).
4. J. Ye, B. Dong, B. Gu, and S. Liu, "Analysis of a cylindrical microlens array with long focal depth by rigorous boundary-element method and scalar approximations," *Appl. Opt.* **43**(27), 5183–5192 (2004).
5. N. Davidson, A. A. Friesem, and E. Hasman, "Holographic axilens: high resolution and long focal depth," *Opt. Lett.* **16**, 523–525 (1991).
6. R. Ponce, A. Serrano-Heredia, and V. Arrizón, "Simplified optimum phase-only configuration for a TNLCD," *Proc. SPIE* **5556**, 206–213 (2004).
7. E. Carcolé, J. Campos, and S. Bosch, "Diffraction theory of Fresnel lenses encoded in low-resolution devices," *Appl. Opt.* **33**(2), 162–174 (1994).
8. V. Arrizón and L. A. González, "Non-paraxial array illuminator based on a single low-resolution pixelated lens," *Opt. Commun.* **199**, 345–353 (2001).
9. J. A. Muñoz-Rodriguez, R. Rodriguez-Vera, and M. Servin, "3-D object profilometry based on direct displacement analysis," *Opt. Eng.* **39**(9), 2463–2471 (2000).
10. S. Ledesma, J. C. Escalera, J. Campos, J. Mazzaferri, and M. J. Yzuel, "High depth of focus by multiplexing annular lenses," *Opt. Commun.* **266**, 6–12 (2006).
11. G. Mikuła, Z. Jaroszewicz, A. Kolodziejczyk, K. Petelczyc, and M. Sypek, "Imaging with extended focal depth by means of lenses with radial and angular modulation," *Opt. Express* **15**(15), 9184–9193 (2007).

Luis A. González received his BS degree in electronics engineering from the Instituto Tecnólogico de Tuxtla Gutiérrez, México, in 1995, and his PhD in optics from the Instituto Nacional de Astrofisica, Optica y Electrónica, México, in 2001. Currently, he is a full-time researcher in the Physics Research Department of the University of Sonora, Mexico. His research interests include spatial light modulators, computer-generated holography, and optical-digital image processing.

Victor Arrizón received his BS degree in physics from the Instituto Politécnico Nacional, México, in 1980 and his PhD in optics from the Instituto Nacional de Astrofisica, Optica y Electrónica (INAOE), México, in 1993. Currently, he works as a full-time researcher in the Optics Department at INAOE. His research interests include spatial light modulators, computer-generated holography, and diffractive optics.